JOURNAL OF GEOPHYSICAL RESEARCH, VOL. 114, A00D02, doi:10.1029/2008JA013849, 2009

Plasma sheet $PV^{5/3}$ and nV and associated plasma and energy transport for different convection strengths and AE levels

Chih-Ping Wang,[1] Larry R. Lyons,[1] Richard A. Wolf,[2] Tsugunobu Nagai,[3] James M. Weygand,[4] and A. T. Y. Lui[5]

Received 23 October 2008; revised 2 January 2009; accepted 6 February 2009; published 18 April 2009.

[1] To understand the large-scale plasma sheet thermodynamics, we have used Geotail data and a formula for estimating flux tube volume V to investigate statistically the equatorial distributions of $PV^{5/3}$ and nV for slow flowing plasma in the nightside plasma sheet and compare them with the physical bases of ideal MHD and the Rice Convection Model (RCM). We have examined the distributions under three conditions: (1) weak convection and low AE, (2) enhanced convection and low AE, and (3) enhanced convection and high AE. The overall nV decreases significantly with increasing convection or AE, while the overall $PV^{5/3}$ remains similar. We found that $PV^{5/3}$ drops significantly earthward along the estimated electric drift paths near midnight, inconsistent with ideal MHD. Examination of $P_kV^{5/3}$ and the electric and magnetic drift paths of different energy invariants, where P_k is the partial pressure of a specific energy invariant, shows that the strong duskward drift of the above thermal-energy particles due to magnetic drift, together with there being significantly fewer higher-energy particles from the dawn flank than from the tail, results in the strong earthward decrease of $PV^{5/3}$. We also found that $d(P_kV^{5/3})/dt = 0$ and $d(n_kV)/dt = 0$ along the electric and magnetic drift paths used in the RCM are good approximations for slow flowing pressure-bearing plasma sheet ions. The distributions of nV indicate that low-energy plasma becomes dominant when convection and AE are low, and their transport from the flanks may be affected by nonadiabatic processes not included in ideal MHD or the RCM.

Citation: Wang, C.-P., L. R. Lyons, R. A. Wolf, T. Nagai, J. M. Weygand, and A. T. Y. Lui (2009), Plasma sheet $PV^{5/3}$ and nV and associated plasma and energy transport for different convection strengths and AE levels, *J. Geophys. Res.*, *114*, A00D02, doi:10.1029/2008JA013849.

1. Introduction

[2] The spatial variations of flux tube particle content nV and the global entropy parameter $PV^{5/3}$are crucial to understanding the thermodynamics of plasma sheet and underlying transport of plasma and energy. Here n is number density, P is plasma pressure, and V is the flux tube volume per unit magnetic flux. Furthermore, how the earthward variation of $PV^{5/3}$ changes in response to enhanced convection is crucial to the stability of the plasma sheet [*Erickson and Wolf*, 1980]. It has been suggested that flux tubes with low $PV^{5/3}$ associated with fast flows drifting from the tail, which are more common when AE is higher [e.g., *Angelopoulos et al.*, 1994], may alter the $PV^{5/3}$ distributions so that the plasma sheet can remain stable under enhanced convection [e.g., *Garner et al.*, 2003; *Wolf et al.*, 2006]. Previous observations have indicated that nV and $PV^{5/3}$ decrease earthward [e.g., *Spence and Kivelson*, 1990; *Kaufmann et al.*, 2004]. However, how the distributions of nV and $PV^{5/3}$ change with the convection strength or with geomagnetic activity has not yet been evaluated. One of our goals in this paper is to determine the earthward variations of $PV^{5/3}$ and nV for different convection strengths and AE levels.

[3] Previous observations [e.g., *Terasawa et al.*, 1997; *Wing and Newell*, 2002; *Tsyganenko and Mukai*, 2003; *Wang et al.*, 2006] have shown that the distributions of plasma sheet number density, pressure, and magnetic fields depend strongly on the interplanetary magnetic field conditions, therefore suggesting that nV and $PV^{5/3}$ may also have a strong dependence on convection strength. However, observational examinations of nV and $PV^{5/3}$ have been rather limited because of the difficulty of estimating V, which relies on a magnetic field model that can provide fields in force balance with the observed P. Recently, algorithms have been developed to utilize large-scale empirical magnetic fields to estimate V from force-balanced

[1]Department of Atmospheric and Oceanic Sciences, University of California, Los Angeles, California, USA.
[2]Department of Physics and Astronomy, Rice University, Houston, Texas, USA.
[3]Department of Earth and Planetary Sciences, Tokyo Institute of Technology, Tokyo, Japan.
[4]Institute of Geophysics and Planetary Physics, University of California, Los Angeles, California, USA.
[5]Applied Physics Laboratory, Johns Hopkins University, Laurel, Maryland, USA.

0148-0227/09/2008JA013849$09.00

magnetic fields using either large-scale 2-D pressure distributions [e.g., *Zaharia*, 2008] or in situ magnetic field and pressure measurements [*Wolf et al.*, 2006]. These algorithms give us the capability to evaluate nV and $PV^{5/3}$ with increased accuracy.

[4] The past theoretical and modeling work on understanding the variations of nV and $PV^{5/3}$ includes whether nV and $PV^{5/3}$ can be conserved for plasma undergoing earthward electric drift to smaller V [e.g., *Erickson and Wolf*, 1980, *Kivelson and Spence*, 1988; *Hau*, 1991], the stability of the plasma sheet [e.g., *Xing and Wolf*, 2007], the effect of magnetic drift [e.g., *Tsyganenko*, 1982; *Spence and Kivelson*, 1990; *Wang et al.*, 2001], the effect of particle source distributions [e.g., *Spence and Kivelson*, 1990; *Wang et al.*, 2001], and changes of particle sources under different interplanetary conditions and geomagnetic activities [e.g., *Garner et al.*, 2003; *Lemon et al.*, 2004]. Two major approximations of the plasma and energy transport behind these theoretical and modeling studies are those of ideal MHD and of the Rice Convection Model (RCM). In ideal MHD, plasma moves along electric drift paths and divergence of heat flux is neglected so that nV and $PV^{5/3}$ are conserved along the drift paths. In the RCM, particles of different energy invariants move along their electric and magnetic drift paths and conserve their total energy, which can lead to divergence of heat flux along total plasma drift paths [*Heinemann and Wolf*, 2001]. The other goal of this paper is to evaluate the extent to which these two approximations can account for the observed variations of nV and $PV^{5/3}$.

[5] In this study, we apply the *Wolf et al.* [2006] algorithm for V to the Geotail observations to examine the distributions of nV and $PV^{5/3}$ and the associated plasma and energy transport under different convection strengths and *AE* levels. We first show how the plasma sheet density, temperature, and pressure change with convection strength and *AE*, and investigate the corresponding changes in magnetic fields and flux tube volumes, as well as the resulting earthward variations of nV and $PV^{5/3}$. To examine the transport of plasma and energy used in ideal MHD and the RCM, we infer electric and magnetic drift from the observed flows, plasma moments, and magnetic fields. We then determine how nV and $PV^{5/3}$ change earthward along electric drift paths and how partial n_kV and $P_kV^{5/3}$ for specific particle energy range k change earthward along the electric and magnetic drift paths.

2. Data

[6] In this study we use Geotail data in aberrated GSM coordinates (with the aberration angle determined by 1 h averaged solar wind velocity) from 1 January 1995 to 31 December 2005 (data from 1996 is not used since there is no *AE* index available for 1996) and in the area $|Y| \leq 20\ R_E$ and $0 \geq X \geq -30\ R_E$ (the smallest radial distance covered by Geotail is $\sim 8\ R_E$). Plasma data from two instruments aboard Geotail are used: the ion and electron data from the Low Energy Particle (LEP) instrument [*Mukai et al.*, 1994] that covers the ion energy range from 21 eV/q to 44 keV/q and the electron energy range from 43 eV to 41 keV, and the proton data from the Energetic Particles and Ion Composition (EPIC) instrument [*Williams et al.*, 1994] that covers the energy range from 46 keV to 3005 keV. Magnetic field data is from the magnetic field (MGF) experiment [*Kokubun et al.*, 1994]. The ion moments are from a summation of the LEP and EPIC data and the electron moments are only from the LEP data. One min averages of the plasma and magnetic field data are used.

[7] The plasma sheet equatorial plane where $B = B_z$ is not the same as the $Z_{GSM} = 0$ plane due to the dipole tilt and motion of the plasma sheet. Thus, to obtain the equatorial distributions of the plasma sheet, we select only data in the region closely surrounding the equatorial plane as defined by plasma pressure ($P_{ion} + P_{electron}$) being larger than magnetic pressure ($P_{mag} = B^2/(2\mu_0)$). We use $V_x > -100$ km/s near typical magnetopause locations to exclude magnetosheath crossings. From each Geotail plasma pressure (P_{ion} from 21 eV to 3005 keV and $P_{electron}$ from 43 eV to 41 keV) and magnetic field measurement, we estimate the plasma pressure and magnetic field strength in the equatorial plane (center of the current sheet), as well as flux tube volume V using a formula based on a simple two-dimensional analytic model of plasma in force equilibrium [*Wolf et al.*, 2006]. The flux tube volume formula performs very well in tests involving force equilibrium magnetic field configurations with a RMS error $\sim$0.16. The estimated V is used only when the perpendicular flow is slow ($V_\perp <$ 150 km/s) and $\sqrt{(B_x^2 + B_y^2)}/B_z \leq 3$, a condition under which *Wolf et al.* [2006] found that their formula provides good estimates.

[8] We use the cross polar-cap potential drop ($\Delta\Phi_{pc}$) to indicate the convection strength. $\Delta\Phi_{pc}$ is estimated using the Weimer empirical model [*Weimer*, 1995], which depends on the IMF B_y, IMF B_z, and the solar wind speed. The Weimer empirical model was established by fitting the coefficients of a spherical harmonic expansion of electric potential to a database with $\sim$1.5 years of electric field measurements from the low-latitude DE2 satellite. The standard deviations of the fitting are $\sim$15 to 18%, indicating that the Weimer model provides quite realistic polar-cap convection patterns and $\Delta\Phi_{pc}$. We used the solar wind and IMF data mainly from Wind. The arrival time of the IMF at the subsolar bow shock at ($X = 17$, $Y = 0$, $Z = 0\ R_E$) is determined by calculating the minimum variance direction using the minimum variance analysis technique [*Weimer et al.*, 2003, 2004]. During times when the Wind data is not available or the propagated Wind data is not reliable because of Wind's position (when Wind is more than $\sim 50\ R_E$ off the Sun-Earth line), we used the solar wind and IMF data from ACE, which is available after February 1998.

[9] Each Geotail observation is associated with the $\Delta\Phi_{pc}$ and *AE* index averaged over the 1 h period prior to that Geotail observation. The data for the central plasma sheet are then sorted into three different conditions, (1) weak convection and low geomagnetic activity: $20 < \Delta\Phi_{pc} < 40$ kV, $AE < 120$ nT, (2) enhanced convection and low geomagnetic activity: $50 < \Delta\Phi_{pc} < 80$ kV, $AE < 120$ nT, and (3) enhanced convection and high geomagnetic activity: $50 < \Delta\Phi_{pc} < 80$ kV, $250 < AE < 500$ nT. (We did not select the condition, $20 < \Delta\Phi_{pc} < 40$ kV and $250 < AE < 500$ nT, because the number of data for this condition is too small.) These criteria were chosen to include sufficient data for

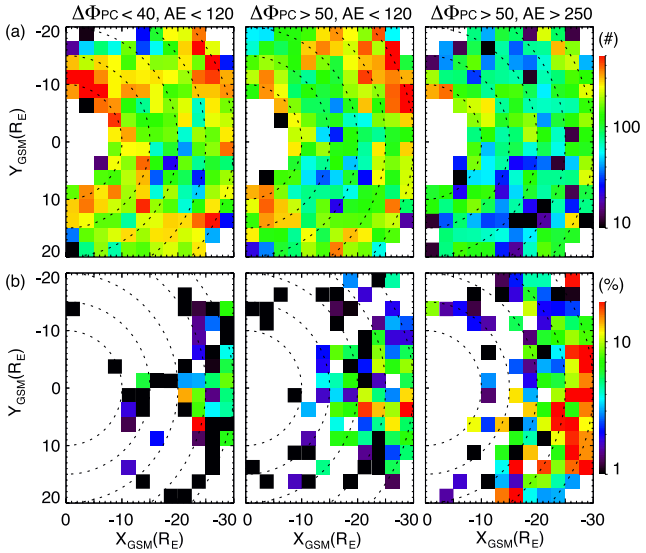

Figure 1. (a) Number of measurements and (b) occurrence frequency (%) of fast flow for the three conditions.

statistically significant results for all three conditions. Finally the sorted data are averaged over 2.5 R_E × 2.5 R_E areas in the $X-Y$ plane according to the X and Y of Geotail. Note that there is a difference between the Geotail (X, Y) and its equatorial mapping location (X_{eq}, Y_{eq}). In this study, we use only data near the equatorial plane and sort the data in 2.5 R_E resolution to minimize the effect of the location difference on the large-scale profiles of the plasma sheet properties.

[10] The numbers of selected data according to the above criteria are shown in Figure 1a. There are more data selected for conditions 1 and 2 than condition 3, likely because of the plasma sheet being relatively thicker for conditions 1 and 2. Figure 1b shows occurrence frequency of fast flows ($V_\perp > 300$ km/s) for the three conditions. It can be seen that fast flows are more frequently observed near midnight and further down the tail. For the same low AE, the frequency increases slightly as $\Delta\Phi_{pc}$ increases and the region where fast flows are observed extends further toward the Earth and the flanks. As both $\Delta\Phi_{pc}$ and AE increase, the fast flow occurrence frequency becomes much higher and the region of large occurrence frequency becomes substantially broader in Y.

[11] To evaluate if our processing of Geotail data described above is capable of revealing the distributions of plasma and magnetic field parameters at the equator, we performed a test using a known force-balanced equilibrium plasma sheet. The equilibrium is obtained by self-consistently modeling the plasma sheet pressure and magnetic fields with 2D force balance maintained around the midnight meridian for two different convection strengths ($\Delta\Phi_{pc}$ = 38 kV and 74 kV) [*Wang et al.*, 2004]. We first established a virtual data set by collecting the pressures and magnetic fields from the equilibrium plasma sheet at all Geotail positions. We then followed the procedures described above to process this virtual data set and compared the results with the equatorial plasma pressure, magnetic field strength, and flux tube volume of the equilibrium plasma sheet. The RMS error at the midnight meridian for $\Delta\Phi_{pc}$ = 38 kV (74 kV) is 7% (11%) for pressure, 16% (10%) for magnetic field, and 6% (12%) for flux tube volume, indicating good accuracy of our data analysis procedure.

3. Results and Analysis

3.1. Equatorial Plasma Moments, Magnetic Fields, Flux Tube Volumes, $PV^{5/3}$, nV, and Their Earthward Variations

3.1.1. Change of the Plasma Sheet Properties With $\Delta\Phi_{pc}$ and AE

[12] Figure 2 shows the equatorial plasma sheet properties during periods of slow flows ($V_\perp < 150$ km/s) under the three conditions and Figure 3 shows comparisons of the X profiles of these properties between the different conditions within three different Y ranges (the midnight sector: $|Y| < 5\ R_E$; the postmidnight sector: $Y < -10\ R_E$, the premidnight sector: $Y > 10\ R_E$). It can be seen from Figure 2 that as $\Delta\Phi_{pc}$ increases and AE remains low (comparisons between conditions 1 and 2), the overall plasma sheet number density (n) decreases but the overall ion temperature (T_i) increases, with these changes being more significant in the midnight sector and at larger radial distance r as shown in Figure 3. The decrease in n but increase in T indicates that the main contribution to the decrease of nV is from loss of colder populations. The decrease in n but increase in T does not result in clear overall changes in pressure. There is only a very slight increase in the ion pressure (P_i), electron pressure (P_e), and the equatorial plasma pressure (P_{eq}) in the midnight sector. It can be seen that in the plasma sheet, P_i is a about a factor of >∼6 larger than P_e, so that ions are the main contributor to plasma sheet plasma pressure. Corresponding to the P changes, both B_{xy} and equatorial magnetic field (B_{eq}) increase and the associated V decreases in the midnight sector between $X \sim -15$ and $-20\ R_E$ with no substantial changes seen in other sectors. As a result, $PV^{5/3}$ increases very slightly in the premidnight sector but decreases in the midnight sector between $X \sim -10$ and $-20\ R_E$. nV decreases everywhere with the decrease being most significant in the midnight sector.

[13] As AE becomes higher and $\Delta\Phi_{pc}$ remains high (comparisons between conditions 2 and 3), a significant decrease in n and an increase in T throughout the plasma sheet can be seen in Figures 2 and 3. P_i, P_e, and P_{eq} also increase everywhere, and the overall increase is larger in the midnight sector. The decrease in n but increase in both T and P indicates a decrease in colder population but increase in hotter population. Correspondingly, B_{eq} becomes stronger throughout the plasma sheet and the increase is larger in the midnight sector. B_{xy}, on the other hand, increases only at larger X in the postmidnight sector, and at smaller X in both the midnight and premidnight sectors as shown in Figure 3. V is seen to decrease throughout the plasma sheet with the decrease being larger in the midnight and postmidnight sectors. The increase of B_{eq} and decrease of V corresponding to the increase of P_{eq} are consistent with results from self-consistent modeling of plasma with force-balanced magnetic fields [e.g., *Lemon et al.*, 2004; *Wang et al.*, 2004]. Despite the large overall increase in P_{eq} and decrease in V, the resulting $PV^{5/3}$ has almost no change in the postmidnight sector and decreases slightly only at smaller X in the midnight and premidnight sectors. The overall decrease in

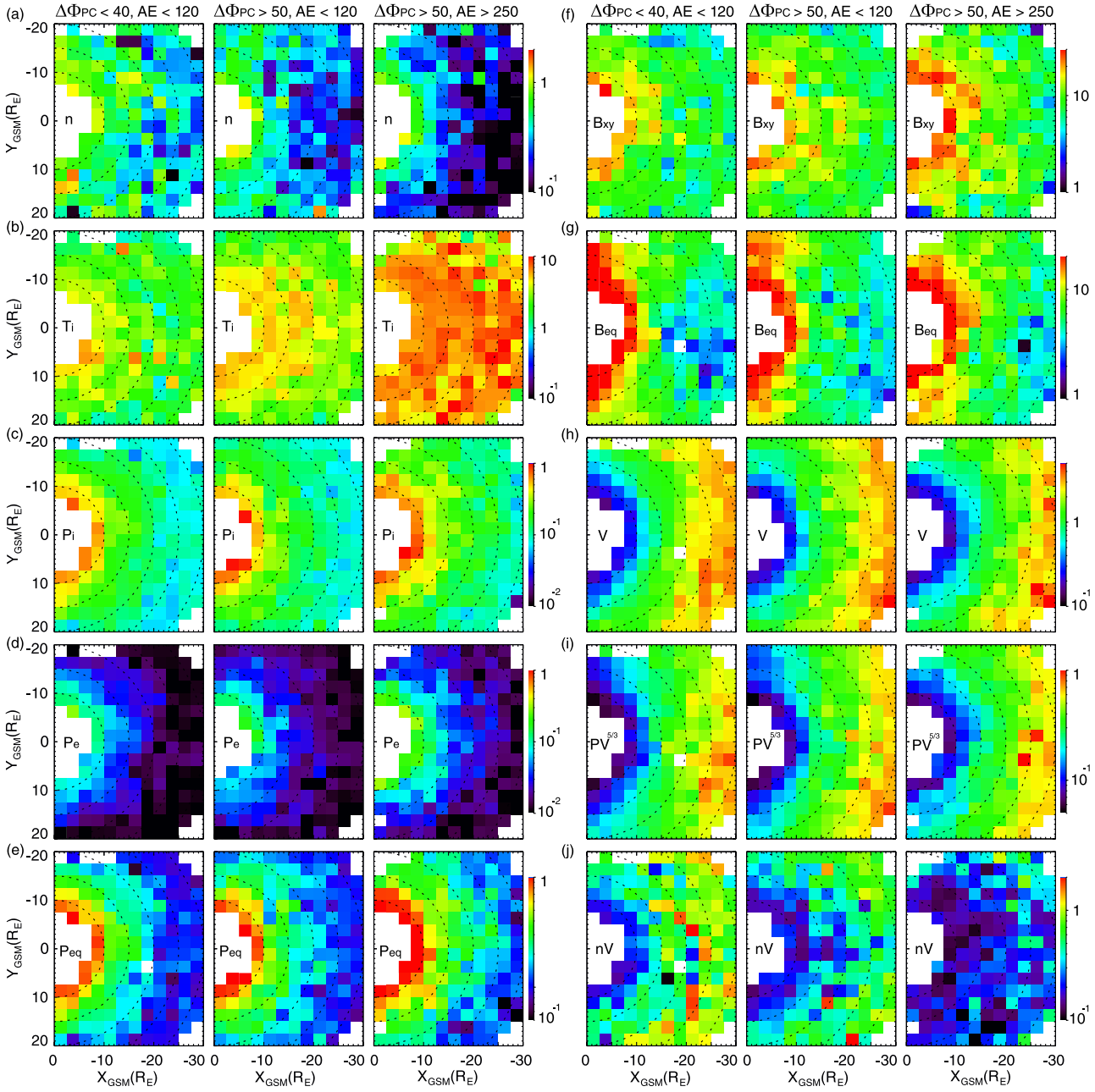

Figure 2. (a) Number density (n, cm^{-3}), (b) ion temperature (T_i, keV), (c) ion pressure (P_i, nPa), (d) electron pressure (P_e, nPa), (e) equatorial plasma pressure (P_{eq}, nPa), (f) plasma sheet $\sqrt{(B_x^2 + B_y^2)}$ (B_{xy}, nT), (g) equatorial magnetic field (B_{eq}, nT), (h) flux tube volume (V, R_E/nT), (i) $PV^{5/3}$ (nPa · $(R_E/nT)^{5/3}$), and (j) nV (cm^{-3} · R_E/nT) for the three conditions.

both n and V, on the other hand, result in a very significant decrease in nV all over the plasma sheet.

[14] The change of the plasma sheet parameters with $\Delta\Phi_{pc}$ and AE is summarized: as $\Delta\Phi_{pc}$ increases (conditions 1 to 2) or AE increases (conditions 2 to 3), decreases are seen in n, V, nV, and $pV^{5/3}$ and increases are seen in T, P_{eq}, and B_{eq} As $\Delta\Phi_{pc}$ increases the changes are mainly seen near midnight and are generally small. As AE increases, the changes are large and are seen throughout the plasma sheet. The dependence of n, T, and P on $\Delta\Phi_{pc}$ are qualitatively consistent with previous observational results of the dependence of these plasma sheet parameters on the interplanetary conditions [*Terasawa et al.*, 1997; *Wing and Newell*, 2002; *Tsyganenko and Mukai*, 2003; *Wang et al.*, 2006].

3.1.2. Earthward Variations of $PV^{5/3}$ and nV for Different $\Delta\Phi_{pc}$ and AE

[15] As shown in Figure 3, n and P increase earthward quite substantially in all Y sectors under all three conditions, while T increases only slightly earthward. These earthward increases are larger in the midnight sector. As $\Delta\Phi_{pc}$ or AE increases, n decreases and T increases, these changes being larger at larger X than at smaller X. As a result, the X profile of n (T) becomes steeper (flatter); however, there is no substantial change in the X profile of P. V decreases

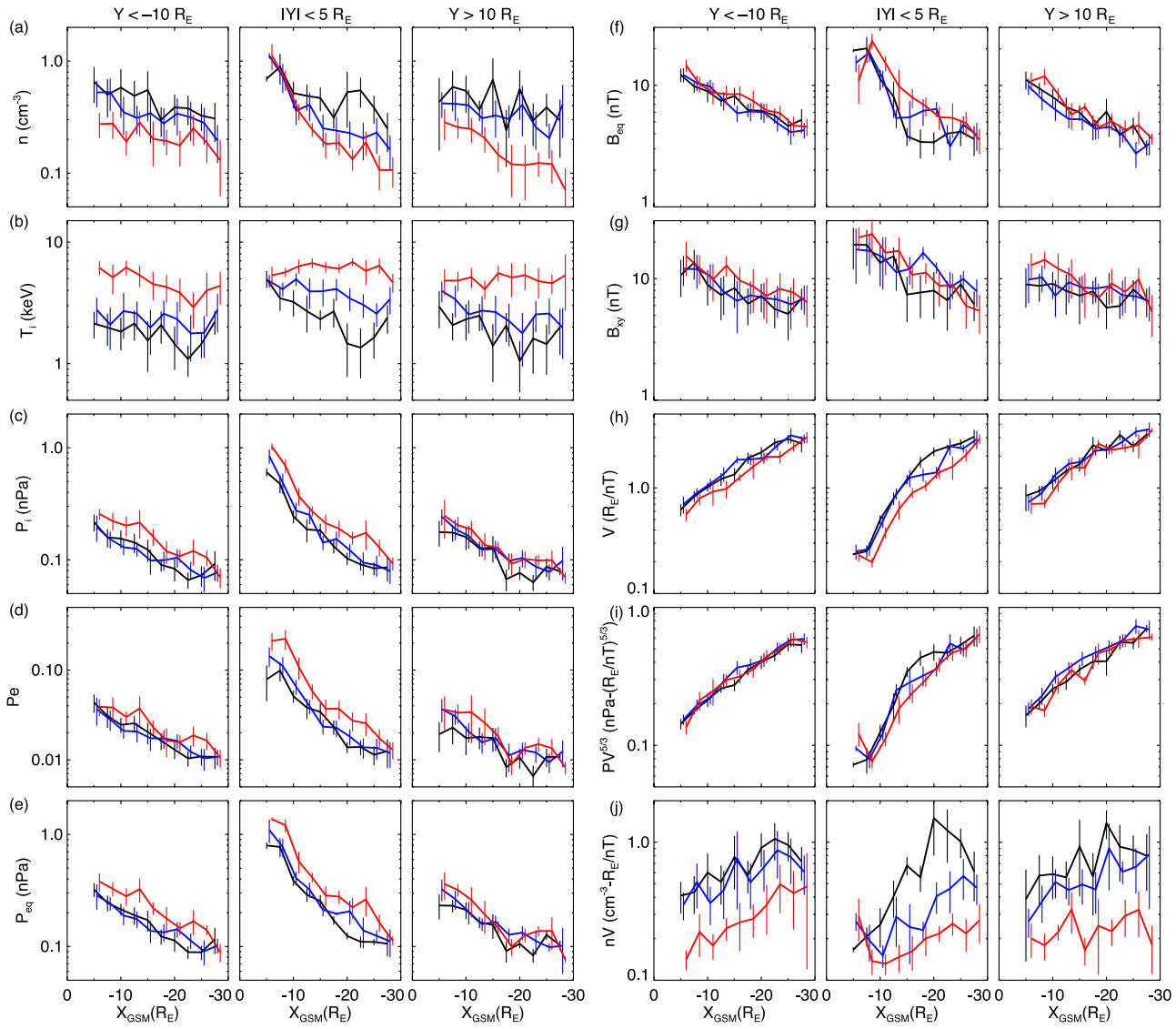

Figure 3. The X profiles of the average of (a) number density (n, cm^{-3}), (b) ion temperature (T_i, keV), (c) ion pressure (P_i, nPa), (d) electron pressure (P_e, nPa), (e) equatorial plasma pressure (P_{eq}, nPa), (f) plasma sheet $\sqrt{(B_x^2 + B_y^2)}$ (B_{xy}, nT), (g) equatorial magnetic field (B_{eq}, nT), (h) flux tube volume ($\mathcal{V}$, R_E/nT), (i) $P\mathcal{V}^{5/3}$ (nPa $\cdot$ (R_E/nT)$^{5/3}$), and (j) $n\mathcal{V}$ (cm^{-3} $\cdot$ R_E/nT) for the three conditions (black curves, condition 1; blue curves, condition 2; red curves, condition 3; vertical lines indicate the standard deviations) within different Y ranges.

earthward more quickly in the midnight sectors than other sectors but its X profile remains unchanged as $\Delta\Phi_{pc}$ and AE change.

[16] The resulting $P\mathcal{V}^{5/3}$ decreases significantly earthward with the decrease being the largest in the midnight sector. Along the midnight meridian, $P\mathcal{V}^{5/3}$ at the tail ($>\sim 25\ R_E$) and near Earth ($<\sim 10$ RE) remain at similar magnitudes but the X profile changes as the condition changes. When $\Delta\Phi_{pc}$ and AE are low, $P\mathcal{V}^{5/3}$ decreases slowly earthward from $X = -30$ to $\sim -15\ R_E$ and then drops more quickly. As $\Delta\Phi_{pc}$ or AE increases, the earthward decrease rate becomes less dependent of X. In the premidnight and postmidnight sectors, the X profile of $P\mathcal{V}^{5/3}$ changes little with the conditions. Therefore, the earthward decrease of $P\mathcal{V}^{5/3}$, from a statistical point of view, does not depend on the convection strength and does not appear to be altered by the presence of more fast flows during high AE as suggested before [e.g., *Garner et al.*, 2003].

[17] Like $P\mathcal{V}^{5/3}$, $n\mathcal{V}$ decreases earthward but with very different rates of decrease for different conditions. In the midnight and premidnight sectors, because $n\mathcal{V}$ decreases more at larger X than at smaller X in response to increasing $\Delta\Phi_{pc}$ and AE, $n\mathcal{V}$ becomes more independent of X when $\Delta\Phi_{pc}$ and AE are high. In the postmidnight sector, $n\mathcal{V}$ decreases but the X profile of $n\mathcal{V}$ does not change much with the conditions.

[18] As $\Delta\Phi_{pc}$ increases and AE remains low, the region of significant decrease in $n\mathcal{V}$ is seen to occur in the midnight sector at larger X. As AE becomes higher under high $\Delta\Phi_{pc}$, the region of significant decrease in $n\mathcal{V}$ is seen to extend further to both the premidnight and postmidnight sectors and smaller X. This is correlated with the region where fast

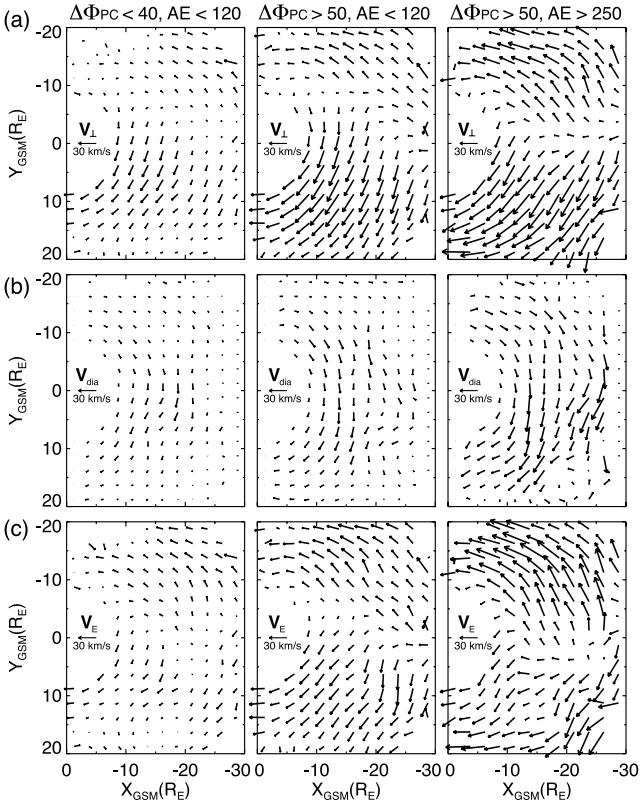

Figure 4. (a) Equatorial perpendicular flow ($\mathbf{V}_\perp$, km/s), (b) diamagnetic drift ($\mathbf{V}_{dia}$, km/s), and (c) electric drift ($\mathbf{V}_E$, km/s) for the three conditions.

flows become more frequent as the condition changes as shown in Figure 1b. However, no such correlation is found between $PV^{5/3}$ and the region of fast flows. As shown in Figures 2 and 3, under all conditions, nV is relatively higher near the flanks than near midnight. As the condition changes, the change in nV is more significant near midnight than near the flanks. Considering that the above nV changes are mainly associated with the cold population and that there are sources for cold particles along the flanks and the source is stronger during northward IMF (low $\Delta\Phi_{pc}$) than during southward IMF (high $\Delta\Phi_{pc}$) [e.g., *Fujimoto et al.*, 1998], it is likely that the change of nV, and maybe also the fast flows, is related to the change in cold populations coming from the flank particle sources.

3.2. Thermodynamics in Ideal MHD and the Rice Convection Model

[19] Ideal MHD and the RCM describe adiabatic plasma transport with different approximations. Ideal MHD assumes that plasma moves with electric drift $\mathbf{V}_E = \mathbf{E} \times \mathbf{B}/B^2$ and that there is no divergence of heat flux and no particle source or loss along flow streamlines. Therefore $d(PV^{5/3})/dt = 0$ and $d(nV)/dt = 0$ along electric drift paths in ideal MHD [e.g., *Heinemann and Wolf*, 2001].

[20] The RCM, under the condition of slow flow, assumes particles of different energy invariants λ_k ($\lambda_k = E_k V^{-2/3}$, where E_k is particle kinetic energy) move with electric and magnetic drift $\mathbf{V}_k = \mathbf{E} \times \mathbf{B}/B^2 + \lambda_k\, \mathbf{B} \times \nabla(V^{-2/3})/qB^2$ and conserve particle number $n_k V$ and energy $e\Phi + E_k$. Therefore $d(P_k V^{5/3})/dt = 0$ and $d(n_k V)/dt = 0$ along the electric and magnetic drift paths [*Wolf*, 1983], where q is particle's electric charge, n_k is partial number density and P_k (= $(2/3)n_k E_k$) is partial pressure for a specific λ_k and energy range, and Φ is electric potential. Note that while particles of each energy invariant are transported adiabatically in the RCM, there is divergence of heat flux when summing up all energy invariants due to energy-dependent magnetic drift [*Heinemann and Wolf*, 2001].

[21] Both ideal MHD and the RCM assume that plasma is isotropic and there is no particle loss and source along the drift paths (though loss processes can be added into the RCM). These are good assumptions for the plasma sheet protons [e.g., *Huang et al.*, 1989; *Kaufmann et al.*, 2002], which contribute to most of plasma pressure as shown in Figures 2 and 3.

[22] Therefore the variations of $PV^{5/3}$ and nV along the $\mathbf{V}_E$ streamlines and changes of $P_k V^{5/3}$ and $n_k V$ along the $\mathbf{V}_k$ streamlines can be examined from our data set to determine the extent of the plasma sheet thermodynamics that can be accounted for by ideal MHD and by the RCM.

3.3. Estimate Electric Drift

[23] Since we cannot obtain electric drift from the Geotail electric field measurement because it is 2D and is only reliable in the duskward component [*Tsuruda et al.*, 1994], we infer electric drift from the flow measurements. In the slow flow approximation plasma drift results from electric drift $\mathbf{V}_E = (\mathbf{E} \times \mathbf{B})/B^2$ and diamagnetic drift $\mathbf{V}_{dia}$, where $\mathbf{E}$ is electric field and $\mathbf{B}$ is magnetic field. $\mathbf{V}_{dia} = (\mathbf{B} \times \nabla P)/(enB^2)$ for protons under the condition of isotropic pressure. Figures 4a and 4b show the observed perpendicular flow $\mathbf{V}_\perp$ (using only $V_\perp < 150$ km/s) and estimated $\mathbf{V}_{dia}$ in the $x - y$ directions, respectively. $\mathbf{V}_{dia}$ is computed using the n, P_{eq}, and B_{eq} shown in Figure 2 with the assumption that all ions are protons. n, P_{eq} and B_{eq} have been smoothed before computing $\mathbf{V}_{dia}$. $\mathbf{V}_E$ is then obtained by subtracting $\mathbf{V}_{dia}$ from $\mathbf{V}_\perp$.

[24] $\mathbf{V}_\perp$ in the tail plasma sheet is generally pointed earthward and duskward (dawnward) in the premidnight (postmidnight) sector with the duskward flows being stronger than the dawnward ones. The duskward flows increase but the dawnward flows decrease with decreasing r. The flow speeds increase as $\Delta\Phi_{pc}$ increases under low AE, and increase more as AE increases. $\mathbf{V}_{dia}$ is mainly azimuthal and directed westward because ∇P_{eq} is mainly in the radial direction. $\mathbf{V}_{dia}$ is stronger near midnight and increases with decreasing r beyond $\sim$10 R_E. $\mathbf{V}_E$ shows earthward and duskward (dawnward) flows in the premidnight (postmidnight) sector. Both $|\mathbf{V}_{dia}|$ and $|\mathbf{V}_E|$ increase with increasing $\Delta\Phi_{pc}$ or AE. Note that $|\mathbf{V}_E|$ is larger when AE is higher even under similar $\Delta\Phi_{pc}$. We computed $\mathbf{E}$ from $\mathbf{V}_E$ and found that $|\mathbf{E}|$ increases with increasing AE under similar $\Delta\Phi_{pc}$, which is also seen in the duskward component of the Geotail electric field measurements (not shown). Both $\mathbf{V}_{dia}$ and $\mathbf{V}_E$ are relatively dawn-dusk symmetric when AE is low but become significantly asymmetric with $\mathbf{V}_{dia}$ ($\mathbf{V}_E$) being stronger in the premidnight (postmidnight) sector when AE is high.

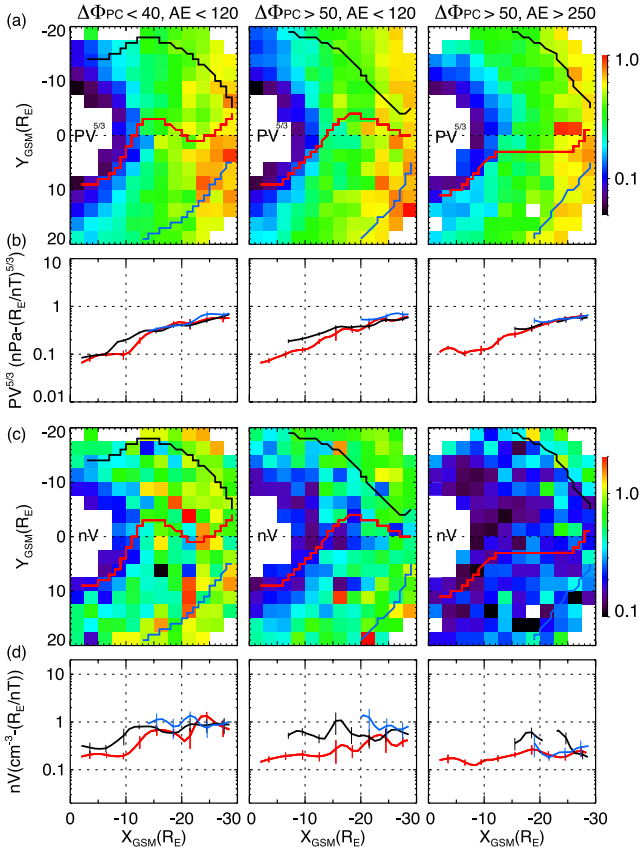

Figure 5. (a) Equatorial $PV^{5/3}$ (nPa · $(R_E/nT)^{5/3}$) superimposed with electric drift paths, (b) X profiles of $PV^{5/3}$ along different electric drift paths, (c) equatorial nV (cm^{-3} · R_E/nT) superimposed with electric drift paths, and (d) X profiles of nV along different electric drift paths for the three conditions.

3.4. The nV and $PV^{5/3}$ Changes Along Electric Drift Paths

[25] As shown in Figures 2 and 3, $PV^{5/3}$ decreases significantly with decreasing radial distance under all three conditions. Figure 5 shows the distributions of $PV^{5/3}$ and nV in the equatorial plane superimposed with the electric drift paths and the variations of $PV^{5/3}$ and nV along the paths. It can be clearly seen that under all conditions the contours of $PV^{5/3}$ do not qualitatively resemble the electric drift paths, while the contours of nV become more similar to the electric drift paths as $\Delta\Phi_{pc}$ and AE increase. $PV^{5/3}$ decreases earthward along electric drift paths and the decrease is most significant (about a factor of ~6 from X = −30 to −10 R_E) along the paths coming from the midnight tail. The $PV^{5/3}$ decrease remains similar as the condition changes. Therefore, the strong decrease of $PV^{5/3}$ along the electric drift indicates that the assumption of $d(PV^{5/3})/dt = 0$ used in the ideal MHD is not appropriate within the $X > -30$ R_E region of the plasma sheet regardless of the convection strength and AE.

[26] Under low $\Delta\Phi_{pc}$ and AE, nV is seen to decrease along the electric drift paths near midnight by a factor of ~5 but fluctuate at similar magnitudes along most portions of the paths away from midnight. As $\Delta\Phi_{pc}$ or AE increases, the nV decreases at larger r but remains similar at smaller r, so that nV changes along the paths around midnight become smaller. Under high $\Delta\Phi_{pc}$ and AE, $d(nV)/dt$ becomes almost zero throughout most of the plasma sheet while $d(PV^{5/3})/dt$ still remains large, indicating that the earthward decrease of $PV^{5/3}$ along the electric drift path is not caused by the earthward decrease of nV.

3.5. The n_kV and $P_kV^{5/3}$ Changes Along Electric and Magnetic Drift Paths of Ions of Different Energies

[27] Figure 6 shows the equatorial distributions of $P_kV^{5/3}$ for ions of different energy invariants λ_k. In defining λ_k (= $E_kV^{-2/3}$), we choose V to be 1 R_E/nT which is the value typically observed at midnight at $X \sim -10$ R_E as shown in Figure 3 so that the value of λ_k (in unit of keV · $(R_E/nT)^{-2/3}$) shown in Figure 6 indicates the particle energy at $X \sim -10$ R_E. Since $P_kV^{5/3} = (2/3)\ \lambda_k nV$, the $P_kV^{5/3}$ distributions are qualitatively the same as those of n_kV for a specific λ_k. It can be seen that the overall $P_kV^{5/3}$ distributions vary significantly with energy. For cold particles with energy well below the thermal energy (see plots of $\lambda_k = 0.6$ for conditions 1 and 2, and $\lambda_k = 0.6$ and 3 for condition 3, since the thermal energy is higher for higher $\Delta\Phi_{pc}$ and AE as shown in Figure 2), $P_kV^{5/3}$ changes more significantly along the Y direction than along the X direction, $P_kV^{5/3}$ being lowest around midnight and becoming higher toward the two flanks. For particles around the thermal energy (see plots of λ_k = 3, 7.5, and 15 for conditions 1 and 2, and λ_k = 7.5 and 15 for condition 3), $P_kV^{5/3}$ is seen to become relatively more constant across the tail and to decrease slightly with decreasing X. For particles that are well above the thermal energy (see plots of $\lambda_k \geq 30$ for all the conditions), $P_kV^{5/3}$ becomes much higher in the premidnight sector than the postmidnight sector and decreases very quickly with decreasing X. The overall magnitudes of $P_kV^{5/3}$ (also n_kV) at lower (higher) energy decrease (increase) significantly as $\Delta\Phi_{pc}$ or AE increases, while the changes of $P_kV^{5/3}$ and n_kV with $\Delta\Phi_{pc}$ or AE for particles around the thermal energy with are relatively smaller.

[28] Figure 6 also shows the drift (electric drift plus magnetic drift, $\mathbf{V}_k = \mathbf{E} \times \mathbf{B}/B^2 + \lambda_k\ \mathbf{B} \times \nabla(V^{-2/3})/qB^2$) paths of λ_k superimposed on the equatorial distributions of $P_kV^{5/3}$ and the variations of $P_kV^{5/3}$ along these drift paths. The drift paths, like the distributions of $P_kV^{5/3}$, change significantly with increasing energy because of the strengthening of magnetic drift. It can be clearly seen that the drift paths for particles above the thermal energy appear to be approximately parallel to the contours of $P_kV^{5/3}$.

[29] For particles well below the thermal energy, their drift is dominated by electric drift. When $\Delta\Phi_{pc}$ and AE are low, $P_kV^{5/3}$ (n_kV) varies substantially along the paths. As $\Delta\Phi_{pc}$ and AE become higher, the changes of $P_kV^{5/3}$ along the paths in the vicinity of midnight become smaller, but along the paths leading toward the flanks $P_kV^{5/3}$ is seen to increase with decreasing X. The variations of n_kV along the drift paths seen at this low-energy range, and how the variations change with $\Delta\Phi_{pc}$ and AE, are very similar to the nV variations along the electric drift paths shown in Figure 5 since low-energy plasma is the main contributor to nV. The strong variations indicate that under low $\Delta\Phi_{pc}$ and

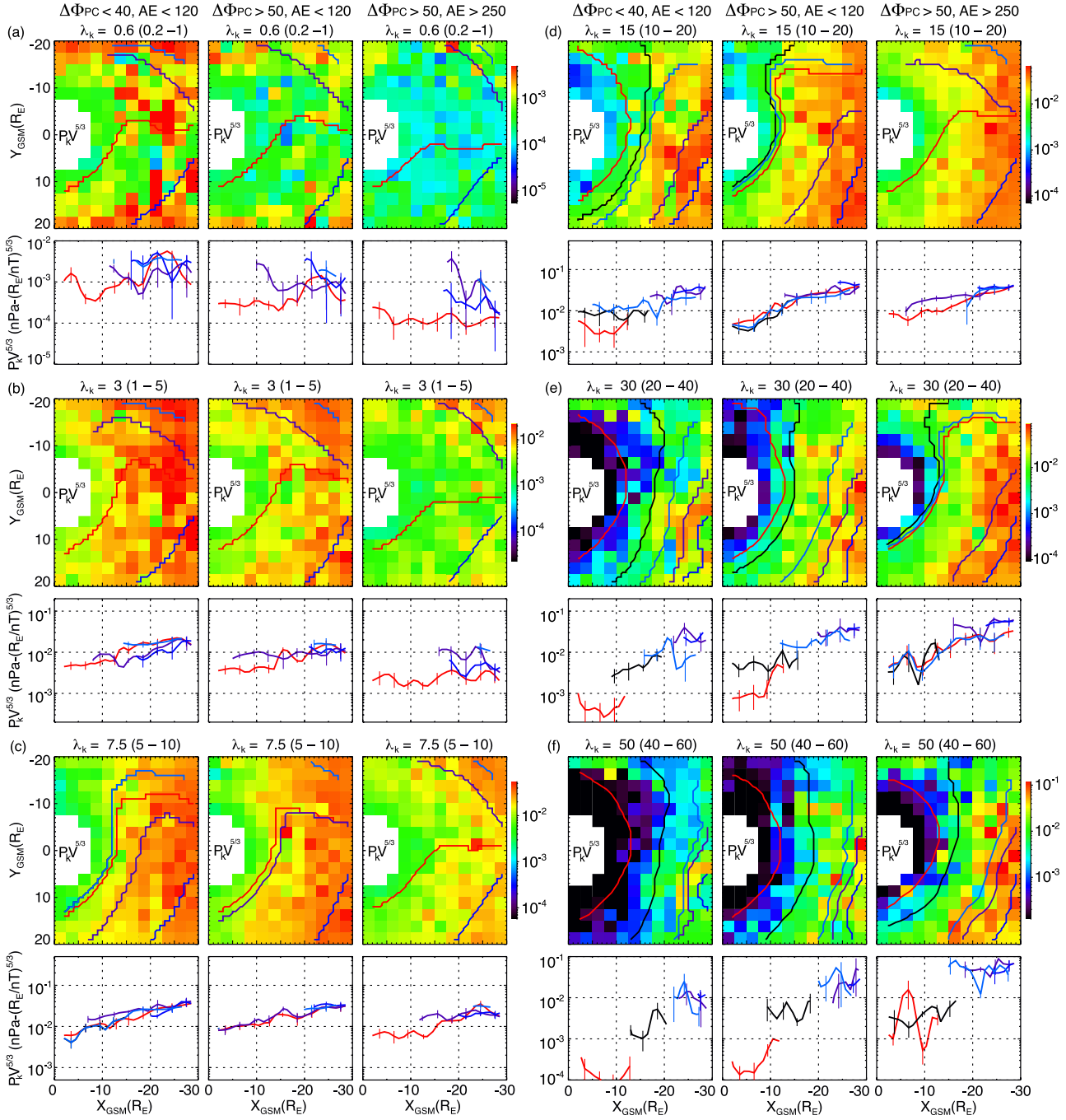

Figure 6. Equatorial $P_k V^{5/3}$ (nPa · $(R_E/nT)^{5/3}$) superimposed with electric and magnetic drift paths and X profiles of $P_k V^{5/3}$ along different electric and magnetic drift paths for different specific energy invariant λ_k (keV · $(R_E/nT)^{-2/3}$) and for the three conditions (the λ ranges for obtaining P_k are indicated by values inside the parentheses) for the three conditions.

AE the RCM cannot account for the $n_k V$ distributions and that the ideal MHD cannot account for the nV distributions.

[30] The above disagreement between the observations and the two models suggests that other processes not included in ideal MHD and the RCM may play an important role in the transport of low-energy particles, one of the possible processes being diffusion [e.g., *Antonova*, 2006]. Considering that cold particles from the tail and from the flanks are transported only by electric drift, the directions of electric drift (earthward and flankward) implies that those cold particles from the tail can have access to most of the plasma sheet while those from the flanks cannot. Therefore, $d(n_k V)/dt = 0$ should be seen throughout the plasma sheet, which is approximately true when $\Delta\Phi_{pc}$ and *AE* are high. When $\Delta\Phi_{pc}$ is low, the number of cold particles along the flanks becomes larger than that from the tail, creating a gradient of number density that points toward the flanks along the Y direction. This gradient favors diffusion that transports cold particles from the flanks toward midnight. When diffusion is stronger than electric drift, a substantial

number of cold particles from the flanks can reach the near midnight region. Therefore, considering diffusion in addition to electric drift can possibly explain the distributions of n_kV for different $\Delta\Phi_{pc}$ and AE.

[31] For plasma around the thermal energy, $P_kV^{5/3}$ is seen to fluctuate and remain at similar magnitudes along most portions of the drift paths or, along a few paths, gradually decrease earthward with the decreases being much less significant (a factor of ~2 to 3 from $X = -30$ to -10 R_E) than the earthward decrease of $PV^{5/3}$ along the electric drift paths shown in Figure 5. As λ_k becomes higher, $P_kV^{5/3}$ has larger fluctuations along the drift paths but still remains at similar magnitudes along those paths that connect to the tail, while the $P_kV^{5/3}$ along the drift paths that connect to the dawn flank changes substantially.

[32] Therefore, $d(P_kV^{5/3})/dt$ and $d(n_kV)/dt$ along the drift paths are not small for low-energy particles. Nevertheless, there is a qualitative similarity between contours of $P_kV^{5/3}$ and drift paths and the $P_kV^{5/3}$ for thermal to high-energy plasma is maintained at similar magnitudes along most portions of the drift paths. These indicate that the RCM physics is appropriate for describing the slow transport of pressure-bearing plasma.

[33] The earthward decrease of $PV^{5/3}$ can be easily understood from the RCM point of view. It can be seen that the thermal and high-energy particles coming from the midnight tail, which are the major contributors to the $PV^{5/3}$, are strongly affected by duskward magnetic drift and are therefore diverted away from the earthward electric drift. In the region of the near-Earth plasma sheet ($X \sim -10$ R_E) near midnight, the high-energy particles are from the dawn flanks. The number of high-energy particles from the dawn flank is considerably lower than that from the tail since the flanks are a source only for low-energy plasma. Therefore, as a result of magnetic drift and uneven spatial distributions of particle sources, $PV^{5/3}$ decreases significantly earthward along midnight. These two factors were also included in the finite tail-width convection model [*Spence and Kivelson*, 1993], which is similar to the RCM in principle.

4. Summary

[34] We have evaluated statistically the spatial distributions of $PV^{5/3}$ and nV in the plasma sheet for different convection strengths and AE levels. We have determined the extent to which that ideal MHD and the RCM can account for the distributions.

[35] We found that the overall nV changes very significantly with convection strength and AE level, while $PV^{5/3}$ only has a slight change mainly near midnight. As the conditions change, the region where fast flows become more frequent is found to be correlated with a significant decrease of nV, but not with the changes of $PV^{5/3}$. Both nV and $PV^{5/3}$ decrease significantly earthward. The earthward decrease of $PV^{5/3}$ remains almost unchanged with the $\Delta\Phi_{pc}$ or AE conditions. The earthward decrease of nV, on the other hand, becomes small as $\Delta\Phi_{pc}$ or AE becomes higher.

[36] $d(PV^{5/3})/dt$ along the electric drift paths is far from zero for all the $\Delta\Phi_{pc}$ and AE conditions, especially near midnight, which is inconsistent with ideal MHD. $d(nV)/dt$ along the electric drift paths is also not zero when $\Delta\Phi_{pc}$ and AE is low, but becomes very small when $\Delta\Phi_{pc}$ and AE are high.

[37] $d(P_kV^{5/3})/dt$ and $d(n_kV)/dt$ along the drift (electric plus magnetic drift) paths are not seen to be small at low energies. Nevertheless, for thermal to high-energy plasma, contours of $P_kV^{5/3}$ can be seen to be roughly parallel to the drift paths and $P_kV^{5/3}$ and n_kV are found to fluctuate but maintain within similar magnitudes along most portions of drift paths. These indicate that the RCM physics is more appropriate than ideal MHD in describing the thermodynamics of slow flowing pressure-bearing plasma, in which magnetic drift plays an important role. Considering that the strength of high-energy plasma source at the flanks is much weaker than that at the tail, the earthward decrease of $PV^{5/3}$ can be understood from the RCM physics.

[38] The overall nV is significantly higher when convection strength and AE level are low because of an increase in cold population. Evaluation of the distribution of the cold population suggests that the plasma sheet under low $\Delta\Phi_{pc}$ and AE is likely to be dominated by low-energy plasma that comes from the flanks, and that their transport toward midnight may be affected by processes not included in ideal MHD and the RCM, such as diffusion.

[39] **Acknowledgments.** The work by C.-P. Wang and L. R. Lyons has been supported by NASA grants NNX07AF66G, NNX07AG42G, and NNX08A135G and NSF grant ATM-0819864. The work by R. A. Wolf has been supported by NASA Heliospheric Theory Program grant NNX08AI55G. The work by J. M. Weygand has been supported by Space Weather grant ATM 02-08501, by NASA Research at 1 AU grant NG-04GA93G, and NASA grant NNX07AC93G. The work by A. T. Lui has been supported by NASA grant NNX07AO88G. We thank T. Mukai at ISAS and CDAWeb for the use of the Geotail LEP data. The Geotail magnetic field data are provided through the DARTS system by ISAS. We thank Jon Vandegriff of the Applied Physics Laboratory for providing the Geotail EPIC data. We also thank Dan Weimer for providing the Weimer variance analysis routine. *AE* index was provided by World Data Center for Geomagnetism, Kyoto.

[40] Amitava Bhattacharjee thanks Nikolai Tsyganenko and another reviewer for their assistance in evaluating this paper.

References

Angelopoulos, V., C. F. Kennel, F. V. Coroniti, R. Pellat, M. G. Kivelson, R. J. Walker, C. T. Russell, W. Baumjohann, W. C. Feldman, and J. T. Gosling (1994), Statistical characteristics of bursty bulk flow events, *J. Geophys. Res.*, *99*(A11), 21,257–21,280, doi:10.1029/94JA01263.

Antonova, E. E. (2006), Quasiturbulent transport and LLBL properties, *Adv. Space Res.*, *37*(3), 532–536, doi:10.1016/j.asr.2006.01.019.

Erickson, G. M., and R. A. Wolf (1980), Is steady convection possible in the Earth's magnetotail?, *Geophys. Res. Lett.*, *7*(11), 897–900, doi:10.1029/GL007i011p00897.

Fujimoto, M., T. Terasawa, and T. Mukai (1998), The low-latitude boundary layer in the tail-franks, in *New Perspectives on the Earth's Magnetotail*, *Geophys. Monogr. Ser.*, vol. 105, edited by A. Nishida, D. N. Baker, and S. W. H. Cowley, pp. 33–44, AGU, Washington, D. C.

Garner, T. W., R. A. Wolf, R. W. Spiro, M. F. Thomsen, and H. Korth (2003), Pressure balance inconsistency exhibited in a statistical model of magnetospheric plasma, *J. Geophys. Res.*, *108*(A8), 1331, doi:10.1029/2003JA009877.

Hau, L.-N. (1991), Effects of steady state adiabatic convection on the configuration of the near-Earth plasma sheet: 2, *J. Geophys. Res.*, *96*, 5591–5596, doi:10.1029/90JA02619.

Heinemann, M., and R. A. Wolf (2001), Relationships of models of the inner magnetosphere to the Rice Convection Model, *J. Geophys. Res.*, *106*(A8), 15,545–15,554, doi:10.1029/2000JA000389.

Huang, C. Y., C. K. Goertz, and L. A. Frank (1989), Observational determination of the adiabatic index in the quiet time plasma sheet, *Geophys. Res. Lett.*, *16*, 563–566, doi:10.1029/GL016i006p00563.

Kaufmann, R. L., C. Lu, W. R. Paterson, and L. A. Frank (2002), Three-dimensional analyses of electric currents and pressure anisotropies in the plasma sheet, *J. Geophys. Res.*, *107*(A7), 1103, doi:10.1029/2001JA000288.

Kaufmann, R. L., W. R. Paterson, and L. A. Frank (2004), Pressure, volume, density relationships in the plasma sheet, *J. Geophys. Res.*, *109*, A08204, doi:10.1029/2003JA010317.

Kivelson, M. G., and H. E. Spence (1988), On the possibility of quasi-static convection in the quiet magnetotail, *Geophys. Res. Lett.*, *15*(13), 1541–1544, doi:10.1029/GL015i013p01541.

Kokubun, S., T. Yamamoto, M. H. Acuna, K. Hayashi, K. Shiokawa, and H. Kawano (1994), The Geotail magnetic field experiment, *J. Geomag. Geoelectr.*, *46*, 7–21.

Lemon, C., R. A. Wolf, T. W. Hill, S. Sazykin, R. W. Spiro, F. R. Toffoletto, J. Birn, and M. Hesse (2004), Magnetic storm ring current injection modeled with the Rice Convection Model and a self-consistent magnetic field, *Geophys. Res. Lett.*, *31*, L21801, doi:10.1029/2004GL020914.

Mukai, T., S. Machida, Y. Saito, M. Hirahara, T. Terasawa, N. Kaya, T. Obara, M. Ejiri, and A. Nishida (1994), The low-energy particle (LEP) experiment onboard the Geotail satellite, *J. Geomag. Geoelectr.*, *46*, 669–692.

Spence, H. E., and M. G. Kivelson (1990), The variation of the plasma sheet polytropic index along the midnight meridian in a finite width magnetotail, *Geophys. Res. Lett.*, *17*(5), 591–594, doi:10.1029/GL017i005p00591.

Spence, H. E., and M. G. Kivelson (1993), Contributions of the low-latitude boundary layer to the finite width magnetotail convection model, *J. Geophys. Res.*, *98*(A9), 15,487–15,496.

Terasawa, T., et al. (1997), Solar wind control of density and temperature in the near-Earth plasma sheet: WIND/GEOTAIL collaboration, *Geophys. Res. Lett.*, *24*(8), 935–938, doi:10.1029/96GL04018.

Tsuruda, K. H., H. Hayakawa, M. Nakanura, T. Okada, A. Matsuoka, F. S. Mozer, and R. Schmidt (1994), Electric field measurements on the GEOTAIL satellite, *J. Geomag. Geoelectr.*, *46*, 693–711.

Tsyganenko, N. A. (1982), On the convective mechanism for formation of the plasma sheet in the magnetospheric tail, *Planet. Space Sci.*, *30*, 1007–1012, doi:10.1016/0032-0633(82)90150-7.

Tsyganenko, N. A., and T. Mukai (2003), Tail plasma sheet models derived from Geotail particle data, *J. Geophys. Res.*, *108*(A3), 1136, doi:10.1029/2002JA009707.

Wang, C.-P., L. R. Lyons, M. W. Chen, and R. A. Wolf (2001), Modeling the quiet time inner plasma sheet protons, *J. Geophys. Res.*, *106*, 6161–6178, doi:10.1029/2000JA000377.

Wang, C.-P., L. R. Lyons, M. W. Chen, and F. R. Toffoletto (2004), Modeling the transition of the inner plasma sheet from weak to enhanced convection, *J. Geophys. Res.*, *109*, A12202, doi:10.1029/2004JA010591.

Wang, C.-P., L. R. Lyons, J. M. Weygand, T. Nagai, and R. W. McEntire (2006), Equatorial distributions of the plasma sheet ions, their electric and magnetic drifts, and magnetic fields under different interplanetary magnetic field B_z conditions, *J. Geophys. Res.*, *111*, A04215, doi:10.1029/2005JA011545.

Weimer, D. R. (1995), Models of high-latitude electric potentials derived with a least error fit of spherical harmonic coefficients, *J. Geophys. Res.*, *100*(A10), 19,595–19,608, doi:10.1029/95JA01755.

Weimer, D. R., D. M. Ober, N. C. Maynard, M. R. Collier, D. J. McComas, N. F. Ness, C. W. Smith, and J. Watermann (2003), Predicting interplanetary magnetic field (IMF) propagation delay times using the minimum variance technique, *J. Geophys. Res.*, *108*(A1), 1026, doi:10.1029/2002JA009405, (Correction, *J. Geophys. Res.*, *109*, A12104, doi:10.1029/2004JA010691, 2004.).

Williams, D. J., R. W. McEntire, C. Schlemm II, A. T. T. Lui, G. Gloeckler, S. P. Christon, and F. Gliem (1994), GEOTAIL energetic particles and ion composition instrument, *J. Geomag. Geoelectr.*, *46*, 39–57.

Wing, S., and P. T. Newell (2002), 2D plasma sheet ion density and temperature profiles for northward and southward IMF, *Geophys. Res. Lett.*, *29*(9), 1307, doi:10.1029/2001GL013950.

Wolf, R. A. (1983), The quasi-static (slow-flow) region of the magnetosphere, in *Solar Terrestrial Physics*, edited by R. L. Carovillano and J. M. Forbes, pp. 303–368, D. Reidel, Norwell, Mass.

Wolf, R. A., V. Kumar, F. R. Toffoletto, G. M. Erickson, A. M. Savoie, C. X. Chen, and C. L. Lemon (2006), Estimating local plasma sheet $PV^{5/3}$ from single-spacecraft measurements, *J. Geophys. Res.*, *111*, A12218, doi:10.1029/2006JA012010.

Xing, X., and R. A. Wolf (2007), Criterion for interchange instability in a plasma connected to a conducting ionosphere, *J. Geophys. Res.*, *112*, A12209, doi:10.1029/2007JA012535.

Zaharia, S. (2008), Improved Euler potential method for three-dimensional magnetospheric equilibrium, *J. Geophys. Res.*, *113*, A08221, doi:10.1029/2008JA013325.

A. T. Y. Lui, Applied Physics Laboratory, Johns Hopkins University, Laurel, MD 20723, USA.

L. R. Lyons and C.-P. Wang, Department of Atmospheric and Oceanic Sciences, University of California, 405 Hilgard Avenue, Box 951565, Los Angeles, CA 90095, USA. (cat@atmos.ucla.edu)

T. Nagai, Department of Earth and Planetary Sciences, Tokyo Institute of Technology, Tokyo 152-8551, Japan.

J. M. Weygand, Institute of Geophysics and Planetary Physics, University of California, Los Angeles, CA 90095, USA.

R. A. Wolf, Department of Physics and Astronomy, Rice University, Houston, TX 77251, USA.